

Scaling Up AI-Generated Image Detection via Generator-Aware Prototypes

Ziheng Qin^{1,2,3*}, Yuheng Ji^{1,3*}, Renshuai Tao², Yuxuan Tian^{1,3}, Yuyang Liu^{1,3}, Yipu Wang^{1,4}, Xiaolong Zheng^{1,3,4,✉}

¹ Institute of Automation, Chinese Academy of Sciences

² Institute of Information Science, Beijing Jiaotong University

³ School of Artificial Intelligence, University of Chinese Academy of Sciences

⁴ School of Advanced Interdisciplinary Sciences, University of Chinese Academy of Sciences

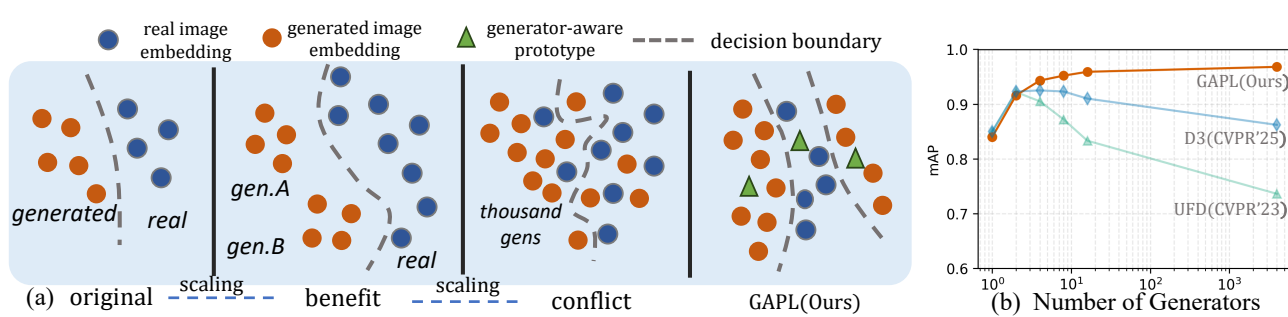


Figure 1. Illustration of the “benefit then conflict” phenomenon we identify. As more generators added to train the detector, it first benefit from the new domain knowledge but eventually degrades due to inseparable embedding. Our proposed method, GAPL, resolves this issue by learning generator-aware prototypes, leading to a substantial mAP improvement over existed detectors in the scaling up settings.

Abstract

The pursuit of a universal AI-generated image (AIGI) detector often relies on aggregating data from numerous generators to improve generalization. However, this paper identifies a paradoxical phenomenon we term the “**Benefit then Conflict**” dilemma, where detector performance stagnates and eventually degrades as source diversity expands. Our systematic analysis, diagnoses this failure by identifying two core issues: severe **data-level heterogeneity**, which causes the feature distributions of real and synthetic images to increasingly overlap, and a critical **model-level bottleneck** from fixed, pretrained encoders that cannot adapt to the rising complexity. To address these challenges, we propose Generator-Aware Prototype Learning (GAPL), a framework that constrain representation with a structured learning paradigm. GAPL learns a compact set of canonical forgery prototypes to create a unified, low-variance feature space, effectively countering data heterogeneity. To resolve the model bottleneck, it employs a two-stage training scheme with Low-Rank Adaptation, enhancing its discriminative power while preserving valuable pretrained knowledge. This approach establishes a more robust and generalizable decision boundary. Through extensive

experiments, we demonstrate that GAPL achieves state-of-the-art performance, showing superior detection accuracy across a wide variety of GAN and diffusion-based generators. Code is available at <https://github.com/UltraCapture/GAPL>

1. Introduction

The increasing sophistication of generative models [3, 51, 69] necessitates the development of reliable AI-generated image (AIGI) detectors to mitigate risks such as misinformation. An ideal detector must generalize to generated images from a wide array of generators. To this end, a common strategy is to expand the training dataset by aggregating data from multiple sources [46, 72] to turn the common *Train on one* to *Train on many*.

However, in the process of directly scaling up existing AIGI detector [45, 72], performance does not always increase as we wish. Instead, we observe a paradoxical phenomenon of **Benefit then Conflict** in scaling up experiments; as illustrated in Fig. 1 while aggregating data from a few generators is beneficial, the detector’s efficacy diminishes as the diversity of training sources expands. This counterintuitive outcome reveals fundamental limitations in scaling current AIGI detectors. To understand the under-

* Equal contribution.

✉ Corresponding author.

lying reason for this phenomenon, we construct a series of datasets equal number of generated images, but varying numbers of generators. Then we use a Linear Discriminant Analysis (LDA) model to assess the intrinsic separability in existing detectors, revealing two conclusions: (1) scaling itself causes data towards inseparable, (2) training in an end to end manner, which thought usually to be overfitting in domain, outperforms pretrained-based ones in scaling up setting. Based on these findings, we identify two primary challenges: **(1) Data-Level Heterogeneity**: The feature distributions of images from different generators are highly diverse thereby amplifying the intrinsic difficulty of the classification task. As shown in Fig. 1(a), this inseparability cause a irregular decision boundary in detectors. **(2) Model-Level Bottleneck**: Many state-of-the-art detectors [36, 45, 57, 68, 70] rely on fixed, pre-trained encoders (e.g., CLIP [49]) for feature extraction. While these models provide powerful semantic priors to achieve generalization when training on single source, these priors may be contradictory when learning from heterogeneous data. As shown in Fig 2, with only one generator, the fixed CLIP embedding space shows a clear decision boundary. However, when the number of generators increases to thousands, the features exhibit significant embedding overlap.

To address these challenges, we pivot from the paradigm of unconstrained data aggregation to a more structured philosophy: *Turn Thousands into a Few*. We realize this through our proposed **Generator-Aware Prototype Learning (GAPL)** framework. Instead of treating all forgery sources equally, GAPL is designed to learn a compact and robust representation of forgery itself. First, to counter *data-level heterogeneity*, it learns a small set of prototypes from a few canonical generators. Each prototype represents a distinct, canonical forgery pattern. **Prototype Mapping (PM)** mechanism integrates prototypes and image embedding by reconstructing the embedding as a linear combination of prototypes weighted by the similarity. This design constrains the feature variance within the range defined by the prototypes, alleviating the heterogeneity of large scale data. Second, to break the *model-level bottleneck*, GAPL adopts a two-stage training scheme that progressively integrates forgery cues into the model while preserving generalization brought by the pretrained encoder as much as possible. In the first stage we only train an MLP to transform the feature space forgery related, in the second stage we use LoRA [25] to tune a low-rank subspace that works synergistically with the PM mechanism. By overcoming the two key challenges, our model establishes a clearer and more generalizable decision boundary. In our comprehensive evaluation across 6 widely used benchmarks encompassing most popular generative models, our detector achieved an average performance of 90.4% and an average accuracy of 94.9%. This outperforms previous SoTA detector by 3.5%.

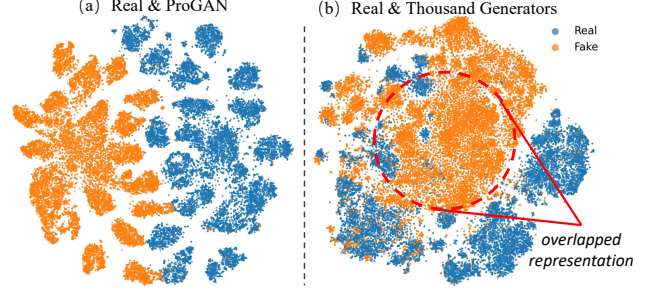


Figure 2. **T-SNE visualization on CLIP Embeddings.** **(a)** Comparison between images generated by a single generator and real images. **(b)** Comparison between images generated by thousands of diverse generators and real images.

Moreover, in-depth experiments demonstrate the excellent robustness of our detector against post processing, thoroughly highlighting its applicability in real world.

Our contributions are summarized as follows:

- We identify and analyze the “Benefit then Conflict” paradox in scaling up setting, revealing the core challenges that impede the scalability of current AIGI detectors.
- We introduce Generator-Aware Prototype Learning (GAPL), a novel framework that effectively manages the high heterogeneity of AI-Generated images by learning a shared space of forgery prototypes.
- Our method overcomes the limitations of fixed feature extractors by explicitly training a model to map diverse artifacts to a set of canonical forgery concepts, enabling a more robust and well-defined decision boundary.
- Through extensive experiments, we demonstrate that GAPL achieves state-of-the-art performance, showing a consistent detection across benchmark with a mean accuracy of 90.4% across 55 test subsets in 6 benchmarks, outperforms existing detectors.

2. Related Works

2.1. Generalized AI-Generated Image Detection

Generalized AIGI detection seeks to train a model that can generalize to unseen generative model from a single training source. The primary approach can be divided into two categories. The first category is to extract a low-level artifact pattern, and detection is via recognizing this artifact pattern. This generalized pattern is from different domains, including data augmentation [65] and local pixel dependency [35, 56] in the common RGB domain. In frequency domain, high frequency component is widely used [26, 34, 55], other domains like reconstruction error [41, 67] and VAE introduced artifact [12, 50] prove that AIGI artifacts widely exist. The second is through semantic-level artifact, based on the fact that generative models often fail to maintain semantic consistency, which can be detected via a pretrained im-

age encoder. UniFD [45] first explored this direction using a frozen CLIP image encoder. Following works exploit the ability of CLIP in AIGI detection via inserting adapter in CLIP [36], creating tunable subspace [71, 73], injecting forgery concept [57] and extract hybrid feature for detection [13, 70]. However, these detectors often fail to maintain consistency performance under domain gap, it's probably because of the fingerprint or inconsistency they aim to extract does not appear in all generative models.

2.2. Curated datasets for AIGI Detection

Existed AIGI detectors were trained on a paired dataset, usually comprise of only one generator or one with its variant [11, 12, 22, 65]. To address the generalization challenges, some efforts have begun attempting the use of data from a more diverse source [68, 70, 72] to build a more convincing detector. However, their approach to curate the dataset is just simply concatenate the existing datasets, which still lacks breadth and diversity. On the other hand, a series of work recognizes the importance of generator diversity, focusing on building large-scale datasets. Specifically, RED series [4, 23] curated datasets from hundreds of generators, while Community Forensics [46] expanded this to the thousand-generator level. These works still leaves a gap: they are either aimed at tasks other than AIGI detection [4, 23], or they train a detector [46] with common vision architecture without specialized design to effectively utilize heterogeneous data. To our knowledge, we are the first to simultaneously consider both model-level and data-level challenges in AIGI detection.

3. Scaling-up AIGI Detectors

In this section, we will delve into the paradox of **Benefit then conflict**, explain how it occurs in scaling up settings in a qualitative way and introduce how the proposed GAPL solves the challenges.

3.1. Challenges in Scaling Up Setting

A common AIGI detector works in the following way. We denote a paired dataset $\mathcal{D} = \{\mathcal{X}, \mathcal{Y}\}$, where \mathcal{X} is the images set $\mathcal{X} = \{x_1, x_2, \dots, x_n\}$, $x_i \in \mathbb{R}^{3 \times H \times W}$ with corresponding label $\mathcal{Y} = \{y_0, y_1, \dots, y_n\}$, $y_i = \{0, 1\}$.

To avoid overfitting, common approach [45, 72] uses an pretrained encoder to extract image embedding $f_i = \phi(x_i) \in \mathbb{R}^D$, where $\phi(\cdot)$ denotes image encoder, and the image embedding refer to its [CLS] token. Subsequently, a classifier \mathcal{G} is applied to predict its log-likelihood, with its parameter θ optimized via cross entropy loss on dataset D :

$$\hat{y} = \mathcal{G}_\theta(f),$$

$$\theta = \arg \min_{\theta} \mathbb{E}_{(x, y) \in D} \left[- (y \log(\hat{y}) + (1 - y) \log(1 - \hat{y})) \right]. \quad (1)$$

Scaling up data itself causes increasing heterogeneity. The discrepancy in the capacity of generative models to approximate the true distribution leads to an increased variance in the combined distribution of different generative models. We consider a dataset distributed according to a gaussian mixture, a series of generative models fit this distribution by maximizing likelihood on this dataset:

$$\begin{aligned} \{x|(x, 0)\} &\sim P_{real} = \sum_k^K \pi_k \mathcal{N}(\mu_k, \Sigma_k) \\ \{x|(x, 1)\} &\sim P_{gen} = \sum_i^G w_i \sum_j^K \pi_{i,j} \mathcal{N}(\mu_{i,j}, \Sigma_{i,j}), \end{aligned} \quad (2)$$

then, according to the law of total variance, the covariance matrix can be calculated with:

$$\begin{aligned} \Sigma_{real} &= \mathbb{E}(\Sigma) + \text{Var}(\mu), \\ \Sigma_{gen} &= \mathbb{E}_G [\text{Var}(X|G)] + \text{Var}_G [\mathbb{E}(X|G)] \\ &= \underbrace{\mathbb{E}_M [\text{Var}(X|G_i, M)|G_i]}_{\text{generator fitting variance}} + \text{Var}_M [\mathbb{E}(X|G_i, M)|G_i] \\ &\quad + \underbrace{\text{Var}_G [\mathbb{E}(X|G)]}_{\text{cross generator variance}}, \end{aligned} \quad (3)$$

where M denotes mode in GMM. The first two terms reflect variance in the learned distribution, which correspond to the terms of the real covariance. The third term, reflects cross generator variance which grows as generator diverse.

To validate our proposal, we conducted an experiment where we collected a series of datasets from GenImage [76]. In each dataset, there are a total number of 8,000 images from ImageNet [16] and the same number of images generated with several models trained on ImageNet, with the number of models varying from 1 to 8. We also uses a dataset with thousands of generative models to further provide large scale setting. For detailed information of these datasets and our experiment, please refer to Appendix A. To estimate the heterogeneity in the dataset, we use scatter matrix of image feature as a proxy for covariance matrix Σ . For a set C , its scatter matrix is calculated by:

$$S = \sum_{f \in C} (f - \mu)(f - \mu)^T, \quad (4)$$

where $\mu = \frac{1}{N} \sum f$ is the mean feature of the extracted features in this set. We calculate the trace of this scatter matrix $tr(S)$ to evaluate total variance of real and generated images.

Results are presented Fig. 3 (a). The figure illustrates that: for the first four datasets, the variance of the generated images exhibits a clear upward trend that scales with the number of generators. Conversely, the variance of real images is highly consistent. In the last dataset, which incorporates real and generated images from diverse sources,

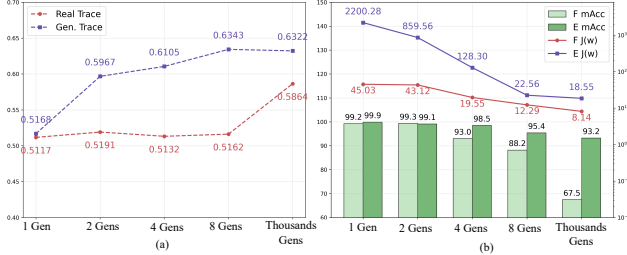


Figure 3. Results of the experiment on a series of datasets comprise of different number of generators. (a) Trace of the scatter matrix from generated images is significantly higher than that from real images. (b) Accuracy of validation and *Fisher ratio* J between end-to-end (E) and frozen-encoder models (F), end-to-end models tend to have a higher separability and accuracy, especially in scaling up settings. “Gen(s)” denotes “Generator(s)”.

the variance of the generated distribution is still markedly higher than that of the real distribution. This confirms our hypothesis: the heterogeneity of real images remain stable whereas the heterogeneity of generated images increases as more generators are introduced.

Reliance on a frozen encoder sets bottleneck to model performance. Common AIGI detectors leverage a pre-trained encoder to avoid overfitting and enhance generalization. This dependency indicates that when training images on novel generators, the model can only push their representations towards the real or generated classes in the feature space, rather than learning the new generative artifacts. This often results in a poor decision boundary and lower discriminability. To investigate the intrinsic discriminability of the feature space, we analyze the embeddings using Linear Discriminant Analysis (LDA) [19]. LDA seeks to create a linear projection space and provides a quantitative measure *Fisher ratio* of this class separability, allowing us to assess how well the pre-trained embeddings can inherently distinguish between real and generated images. Moreover, its optimization can be given in closed form:

$$\begin{aligned} w &= \arg \max_w J(w) = \frac{w^T S_b w}{w^T S_w w} \\ &= k S_w^{-1} (\mu_0 - \mu_1), \end{aligned} \quad (5)$$

where S_b, S_w are scatter between classes and within class matrices, respectively, which can be calculated by

$$\begin{aligned} S_w &= \sum_{i=0}^C S_i \\ S_b &= (\mu_0 - \mu_1)(\mu_0 - \mu_1)^T \end{aligned} \quad (6)$$

We designed an experiment with the datasets introduced above in the following steps: (1) For each dataset, train an

end-to-end classifier, simultaneously, train a classification head based on an frozen image encoder of CLIP. (2) Extract penultimate representation from the two models on validation set, estimate J based on eqs. (5) and (6) and classify them with a threshold of 0.5. We report detection accuracy and *Fisher ratio* J as metrics.

The results are presented in Fig. 3(b). Results reveal that first, *Fisher ratio* and detection accuracy drops as more diverse data adds. Second, an end-to-end detector has a higher *Fisher ratio* on the same data scale compared to the pretrained-based one. Although they achieve good generalization by training on single source with a relatively small *Fisher ratio*, they seemed to be indistinguishable to more generators. This lead us to reflect that the reliance of pre-trained encoder in prevalent AIGI detectors may fundamentally impose an upper bound on achievable performance when scaling up AIGI detection.

3.2. Scaling Up with Generator-Aware Prototypes

Up to now, we have identified key challenges in building a scaling up AIGI detector: (1) To lower inner heterogeneity of generated images, we need to achieve a compact representation for the generated images. (2) Fixed embedding space should be abandoned. Relying on a static embedding space like a frozen CLIP is fundamentally limiting.

To tackle the two challenges, we propose GAPL for scaling up AIGI detection. we adopt a philosophy called *Turn Thousand into a Few*, the GAPL learns a compact shared prototype space to distill thousands of generators into a few, representative prototypes. This process is via a two-stage learning framework, we first leverage pretrained encoder to construct prototype, then we let prototypes guide the encoder to learn and project to this prototype space. The framework of GAPL is shown in Fig. 4.

STAGE I: Creating Forensic-Realated Space and Generator-Aware Prototypes.

The objective of this stage is to perform a supervised projection, creating a forgery-related subspace based on the pretrained embedding space. Since most pretrained encoder are highly correlated with semantic information due to its pretraining objective, we aim to endow the encoder with a basic understanding of generated images, enabling it to capture representative concepts.

Specifically, We select an amount of M images each from ProGAN[31], Stable Diffusion v1.4 [51], and Midjourney [1], sourced from the ForenSynths [65] and GenImage [75] as they represent GANs, Latent diffusion models and Commercial APIs to form a prototype set. We also pair the same amount of real images accordingly. Then, an MLP was attached after the encoder to project dimension and get logits for classification, the projection and MLP can be formulated with $g_{proj} : \mathbb{R}^D \rightarrow \mathbb{R}^{D'}$ and $\text{MLP} : \mathbb{R}^D \rightarrow \mathbb{R}$. This

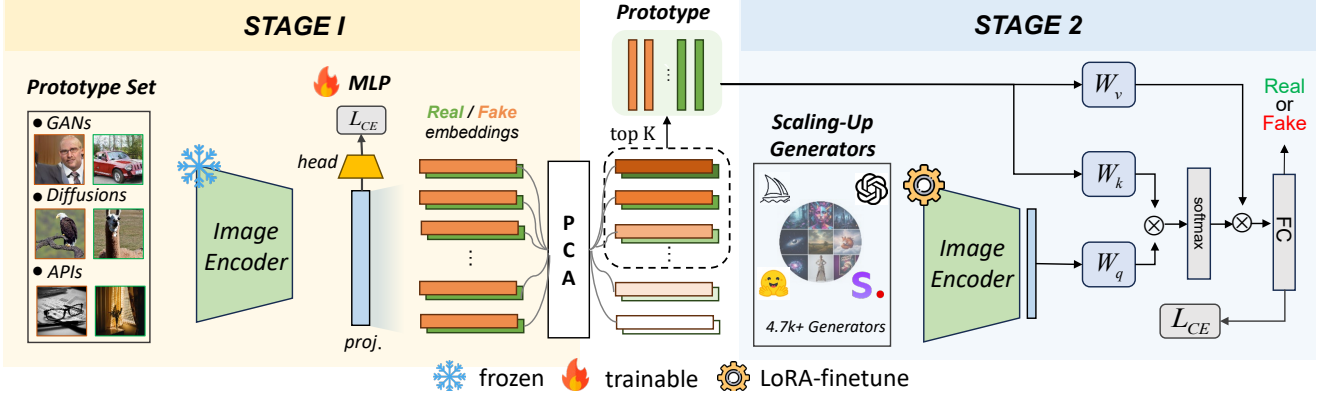


Figure 4. **The overall framework of our GAPL.** We train the GAPL in two stages. In the first stage, we train a MLP and extract embeddings for PCA decomposition, we only retain top N components as prototypes; in the second stage, we use LoRA to finetune the encoder and map image embedding to prototypes to get the final logits.

process can be formulated as follow:

$$\begin{aligned} f &= \phi(x), \\ \hat{y} &= \text{MLP}(\text{Normalize}(f)), \end{aligned} \quad (7)$$

where $\phi(\cdot)$ is the image encoder. In the first stage, the image encoder keeps frozen, we only train this MLP with binary crossentropy as loss function on the prototype set.

Subsequently, we utilize the intermediate layer of the MLP to extract forgery-related embeddings to build prototypes. $\mathbf{F}_f = [f_1^f, f_2^f, \dots, f_{M \times 3}^f]$, $\mathbf{F}_r = [f_1^r, f_2^r, \dots, f_{M \times 3}^r]$, $f \in \mathbb{R}^{D'}$, denotes the real and generated subset of these embeddings. We then perform principle component analysis (PCA) separately on the two subsets for prototype constructing, and select the top $N/2$ principal components from each subset as Generator-Aware Prototypes:

$$\begin{aligned} C &= \frac{1}{3M-1} (\mathbf{F}_f - \mathbf{1}\bar{\mu})^T (\mathbf{F}_f - \mathbf{1}\bar{\mu}), \\ Cv_i &= \lambda_i v_i, \\ \mathbf{P}_f &= [v_1, v_2, \dots, v_{N/2}]^T \in \mathbb{R}^{(N/2) \times D'}, \end{aligned} \quad (8)$$

where $\bar{\mu} \in \mathbb{R}^{1 \times D'}$ is mean vector of the embeddings in \mathbf{F} . $\mathbf{1}_{3M}^T \in \mathbb{R}^{3M}$ denotes all-one vector. We concatenate real and generated prototypes to form the final prototype matrix $\mathbf{P} = [\mathbf{P}_r; \mathbf{P}_f] \in \mathbb{R}^{N \times D'}$.

We adopt this selection strategy based on the assumption that, PCA decomposes the covariance matrix, the components with larger variance capture more general forgery-related information, while those with smaller variance reflect generator-specific characteristics. The remaining components, which contribute little to the overall variance, are mainly task-irrelevant noise and thus discarded.

STAGE II: Map Generators to Prototypes for Large Scale AIGI Detection. In the second stage, we further enhance the model's capability, adhering to our principle of

not relying on a fixed embedding space. To maintain as much knowledge as possible in pretrained image encoder, this adaptation is performed using LoRA [25].

$$f = g_{proj}(\phi_{lora}(x)). \quad (9)$$

Furthermore, we aim to solve how to effectively integrate the extracted prototype with the image feature from image encoder. Given that our primary objective is to enforce feature in a low variance way, we posit that a good approach is to represent each image's features into a dynamic linear combination of these learned prototypes. It should create a map from the diverse feature space onto a low-variance prototype space. Therefore, we adopt a simple yet effective cross-attention [64] mechanism as this mapping to perform feature fusion, where the image embedding act as queries and the prototypes serve as keys and values. It can be expressed as follows:

$$\begin{aligned} \tilde{f} &= \text{Attn}(W_q f, W_k \mathbf{P}, W_v \mathbf{P}) \\ &= \text{softmax}\left(\frac{(f W_q)(\mathbf{P} W_k)^T}{\sqrt{D'}}\right) \cdot \mathbf{P} W_v \end{aligned} \quad (10)$$

Where $W_q, W_k, W_v \in \mathbb{R}^{D' \times D'}$ is the respective affine matrix. We feed this re-organized feature \tilde{f} into a linear classifier to predict its final logits and train the whole model with binary crossentropy.

4. Experiments

In this section, we evaluate the proposed GAPL to validate the following **Research Questions (RQs)** :

- RQ.1: How well does the proposed **GAPL** in detecting generated images from any generator?
- RQ.2: How well is the inherent potential of proposed **GAPL** in model architecture?

Method	Training Class/Num.	ForenSynths		UFD		GenImage		SynthBuster		Chameleon		CommFor		Mean	
		Acc	AP	Acc	AP	Acc	AP	Acc	AP	Acc	AP	Acc	AP	Acc	AP
<i>GAN-Generalized</i>															
CNNDet [65]	ProGAN/720k	75.3	91.8	53.1	71.1	51.3	65.6	50.3	53.9	57.0	42.6	51.5	53.7	56.4	63.1
NPR [56]	ProGAN/144k	90.8	91.8	95.1	97.4	86.2	91.6	38.9	45.4	57.4	47.7	73.8	74.7	73.7	74.8
UniFD [45]	ProGAN/720k	89.4	96.7	82.2	95.7	70.0	88.3	67.6	78.0	57.2	46.2	54.0	58.3	70.1	77.2
SAFE [34]	ProGAN/144k	96.2	98.6	95.7	99.1	95.5	99.3	44.7	44.7	59.2	50.6	50.0	48.3	73.6	79.2
AIDE [70]	ProGAN/720k	88.4	96.0	96.7	99.0	92.0	97.5	48.0	49.9	58.4	50.1	49.9	47.1	72.2	73.3
<i>Diffusion-Generalized</i>															
DRCT [11]	SD2.1/473k	50.0	49.7	70.0	79.2	78.0	94.0	77.6	84.7	79.8	85.2	49.6	49.4	67.5	73.7
Co-SPY [13]	SD1.4/320k	65.6	75.9	76.8	84.3	78.0	94.1	77.4	91.6	68.8	68.8	67.9	79.2	72.4	82.3
B-Free [22]	SD2.1/360k	81.1	94.2	87.1	95.3	87.3	97.7	94.9	98.8	<u>78.2</u>	<u>85.2</u>	81.5	91.8	85.0	93.8
<i>Scaling-Ups</i>															
AIDE [70]	8gens/1.3M	85.3	93.8	98.5	99.9	99.7	100.0	52.7	56.0	65.8	69.7	50.1	48.2	75.4	77.9
D3 [72]	9gens/2M	93.0	97.9	94.8	99.0	95.4	99.2	81.3	89.5	61.0	56.5	73.6	86.0	83.2	88.0
CommForen [46]	4.7Kgens/5M	92.3	98.2	94.0	97.0	84.0	93.4	87.0	94.7	77.5	83.5	<u>86.8</u>	<u>93.9</u>	<u>86.9</u>	<u>93.4</u>
GAPl(Ours)	4.7Kgens/550k	97.2	99.5	<u>97.2</u>	<u>99.8</u>	<u>96.7</u>	<u>99.6</u>	<u>91.1</u>	<u>97.2</u>	71.0	75.6	89.4	97.8	90.4	94.9

Table 1. Overall performance of different detectors across benchmarks. *GAN-Generalized* means that these models were trained on GAN-generated images, *Diffusion-Generalized* means diffusion-generated images accordingly. *Scaling-ups* means that these model have the access to all kinds of images. We also report each detector’s generator type and number of images of their training set.

- RQ.3: Why is the designed Prototype Learning and two-stage training useful?
- RQ.4: How does the number of prototypes and selection of prototype sets affect performance?
- RQ.5: How well is the proposed **GAPl**’s robustness in handling post processing?

4.1. Experiment Details

Traning set. In our GAPl, prototype set and scaling up set are used for training. In the prototype set used in first stage, we select $M = 2000$ images generated by ProGAN [31], SDV1.4 [51] and Midjourney [1]. These images are sampled from Forensynths and GenImage. As for scaling up dataset, we choose the Community-Forensic [46]. This dataset manually chose 12 GANs, 3 pixel diffusion models and collected about 4000 latent diffusion models on huggingface, constituting a large and diverse datasets that covers most generative architectures. We uses a small version, compared to the original dataset of 5.4M images, the small version only contains 550k images while the total number of generative models remains the same.

Testing set. We select six benchmarks to evaluate our method’s generalization, covering a spectrum of common and advanced generative models developed over the last decade. Tab. 2 lists some information about the benchmarks. Note that despite the use of a large scale training set, more than half of generative models in testing set are still unseen by the detector. See Appendix. B for detailed introduction of these benchmarks.

Dataset	#Real/#Fake	# Models	Type of models
Forensynths [65]	31k/31k	8	GAN
UniversalFakeDetect [45]	8k/8k	8	Diffusion
GenImage [76]	48k/48k	8	GAN&Diffusion
Synthbuster [7]	1k/9k	9	Diffusion
Chameleon [70]	14.9k/11.2k	-	Unknown
Community-Forensics Eval [46]	25k/25k	21	Diffusion

Table 2. The selected 6 AIGI benchmarks to evaluate the methods.

Implementation Details. We use the image encoder of CLIP-ViT:L [18, 49] for finetuning. We select $M = 2000$ images each from 3 generators as prototype set, along with the same amount of real images. The dimension of projection is set to be $D' = 128$, and the number of prototypes is $N = 64$. The experiment was conducted on 2 GeForce RTX 4090 GPUs. More details are in Appendix. E

4.2. Comprehensive evaluation of detection performance across generators (RQ.1)

To evaluate the overall detection performance of the proposed GAPl, we conduct test on the 6 selected benchmarks. The results are shown in Tab. 1. The results reveal the following: **(1) Generalized AIGI detectors fail to maintain performance.** Generalized detectors can achieve a promising performance on only one or two benchmarks. Detectors like SAFE [34], achieve an over 95% accuracy on the previous 3 benchmarks, but fails on the latter 3 with about 50% accuracy, which demonstrates that it is hard to build a well generalized detector on one training source. **(2) GAPl**

Method	Venue	FS	UFD	GI	SB	Mean
<i>General Vision Models</i>						
ResNet [24]	CVPR2015	73.8	79.9	66.4	73.0	73.3
CLIP:ViT [49]	ICML2021	78.3	74.8	73.8	65.8	73.2
ConvNext [38]	CVPR2022	94.5	93.7	85.7	70.8	86.2
Swin-T [37]	ICCV2021	93.3	95.6	89.8	80.2	89.7
<i>AIGI Detectors</i>						
Co-SPY [13]	CVPR2025	49.4	50.0	51.9	50.0	50.4
PatchForen [10]	ECCV2020	54.4	55.0	50.7	60.6	55.2
NPR [56]	CVPR2024	51.1	57.5	56.4	56.5	55.4
UniFD [45]	CVPR2023	62.4	50.1	63.6	63.3	59.8
D3 [72]	CVPR2025	75.0	57.0	59.2	72.2	65.9
Effort [71]	ICML2025	84.4	66.3	71.4	88.0	77.5
AIDE [70]	ICLR2025	86.8	90.5	96.6	67.0	85.2
GAPL (Ours)	-	97.2	97.2	96.7	91.1	95.5

Table 3. Comparison on different model architecture. We reimplement these detection method on exactly the same data as ours, including prototype set and scaling up set and report their binary accuracy and mean accuracy on 4 benchmarks.

exhibits consistent and promising performance. The proposed GAPL achieves a 90.4% average accuracy across 55 test subsets in 6 benchmarks, with a 3.5% average accuracy improvement over the previous detectors. Additionally, we reach a 94.9% average precision and over 90% mAP in most benchmarks, which further validates our promising detection against generated images.

4.3. Cross-Model Comparison in scaling up setting (RQ.2)

To ensure fair comparison and evaluate the inherent ability of the proposed architecture, we conduct an experiment where all methods are trained on the same dataset with ours. Apart from AIGI detectors, we also select some general vision models, including CNN-based [24, 38] and Transformer-based [37, 49] as baselines. The results in Tab. 3 reveal the following: **(1) GAPL has the best mean performance in scaling up setting.** Among the all detectors, GAPL was the best in terms of accuracy. This indicates our design, integrating priors of pretrained encoder and forgery-related knowledge, is beneficial in scaling up setting. **(2) Common AIGI detectors perform even worse when data scales.** Previous AIGI detectors not only perform worse than general vision models, but also worse than the counterpart that trained on single source. This indicates that previous AIGI detectors are often tailored to specific artifact (e.g VAE decode artifact), rendering them ineffective at scale where diver generative model dilute these priors.

4.4. Effect of the designed modules (RQ.3)

To evaluate the impact of the designed modules, we conduct ablation studies on the three components in the proposed

Group	Module			Metrics	
	PCA	PM	LoRA	MAcc	MAP
1	✗	✗	✗	60.05	66.07
2	✗	✓	✗	68.59	72.43
3	✗	✗	✓	88.52	97.91
4	✓	✓	✗	71.88	82.18
5	✗	✓	✓	90.35	95.40
Ours	✓	✓	✓	95.54	98.97

Table 4. Ablation study regarding the designed modules. All the results reported are mean of the 4 benchmarks.

GAPL: (PCA) creating extracting prototype from generator via PCA, prototype matching via cross attention (PM) and LoRA finetuning. The results are shown in Tab. 4. From the results, we can infer that: **(1) PCA proposed in STAGE I effectively extracts generator-aware concepts.** Compare performance in group 1,2 and 4, prototype mapping gain an accuracy performance by 8.54% while PCA further improves 3.28% by injecting concepts related to generators. **(2) PM and LoRA work cooperatively to effectively inject large scale generative knowledge to pretrained encoder.** By comparing the performance of group 2,3 and 5, we observe a gradual performance improvement. This indicates that while the PM module provides the core structure for prototype matching, LoRA finetuning is also essential to adapt encoder to this prototype space, enabling it to effectively align with the extracted generator-aware prototypes.

4.5. Exploration of selecting Prototype Set (RQ.4)

To explore the influence of the number of prototypes retain in PCA and the selection of prototype set, we conduct experiment in multiple group of settings. The results are presented in Fig. 5. Results reveal that: **(1) Number of prototypes slightly affect performance.** Model performance slightly improves as N increases, starting from 16 prototypes with a 95.28% accuracy, keep doubling the number improves it by 0.03% and 0.23%. **(2) More generator to build prototypes yield performance gains.** Randomly generating some prototype vector has a performance of 90.35%, while adding more generator gains performance by 3.22%, 0.42% and 1.44%. But as we try to add generators, the performance goes down, this indicates that the “a few” in *turn thousand into a few* should not be too many, three or four is abundant for the model to adjust.

4.6. Evaluation on robustness (RQ.5)

To validate the robustness of our model against post-processing operations, which are commonly encountered in real-world scenarios, we conduct a robustness evaluation on JPEG compression and Gaussian blur. We select some com-

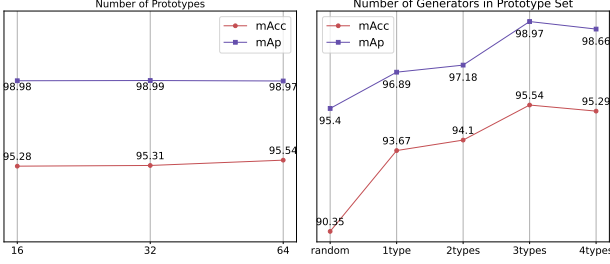


Figure 5. Ablation study regarding the strategy of extracting prototypes. We compare number of prototypes retain in PCA and types of generators in Prototype Set.

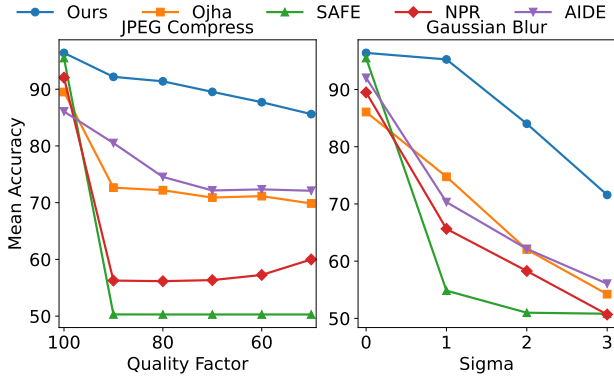


Figure 6. Comparison of **Robustness performance** regarding post process on GenImage dataset. Our model achieve the best overall performance on post process with the minimum degradation.

mon AIGI detectors on GenImage dataset as baselines, to align the performance of starting point, we select checkpoints trained on GenImage SD1.4 subset for these baselines. Results in Fig. 6 shows that: (1) **GAPL keeps steady performance with minimum degradation**. The proposed GAPL not only retains the best overall performance but also has an degradation of only 11.09% and 25.12% in extreme JPEG compression and gaussian blur. (2) **Frequency based AIGI detectors suffer from post process**. Detectors that leverage frequency domain information like AIDE and SAFE behave bad in JPEG compress experiments, a slight JPEG compression could affect the performance to almost random choice of 50%. This also suggests that these detectors are unreliable in real life scenarios.

4.7. Visualization on learned prototypes

To validate **how our model utilizes prototypes**, we calculate the average attention scores between prototypes and images on the validation set, we plot the results in Fig. 7. From the figure, (1) **certain prototypes are consistently utilized by the model**. This indicates that some pattern were common in generated images and real images. Subsequently, to uncover what hide behind these frequently utilized pro-

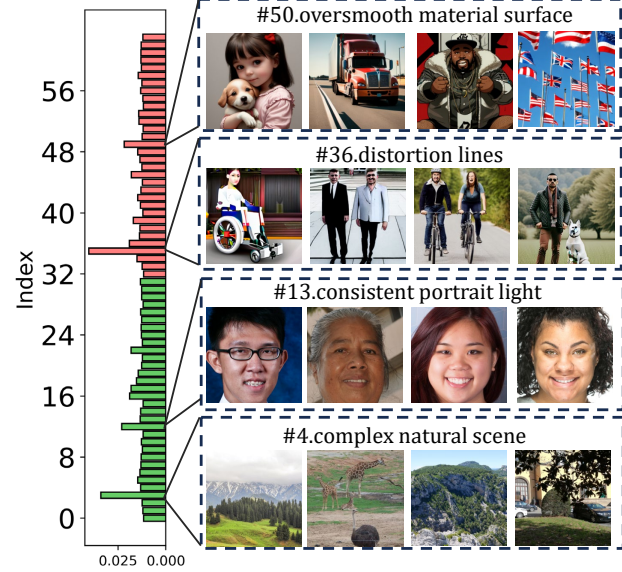


Figure 7. **Average attention scores** on the validation set. Column in red and green means prototypes extracted with real images and generated images, respectively. We collected images that exhibit high attention score for a specific prototype and discovered that they have visual features in common.

totypes, we clustered the images that exhibited particularly high attention scores for a specific prototype. We find that (2) **images pay extreme attention to a certain prototype share some visual characteristics**. In generated images, those feature distorted objects and unrealistic lines pay high attention to Prototype #36, images pay attention to Prototype # 50 usually contain over smooth material surface. As for real images, complex natural scene and consistent portrait light make them look real, which frequently exist in clusters of Prototype #4 and Prototype #13. This finding indicates that our method indeed learned some sort of pattern and the mapping between image with these prototypes.

5. Conclusion

In this paper, we investigate the scaling up setting in AI-Generated Image detection. We first analyze the challenges in scaling up AIGI detector, limitations in existing detectors. Accordingly, we propose GAPL to solve the challenges. It's designed to effectively exploit the data from diverse generators. Extensive experiments demonstrate that scaling up training is crucial for building a detector that generalizes well to detect diverse generative models and our method achieving consistent performance in this setting, paving the way towards a universal AIGI detector.

Limitation. The method proposed in this paper achieves a consistent and generalized performance across existing benchmarks. But we are still unable to definitively assess

the model’s performance when confronted with completely unknown domain, such as images generated from the next generation generative models that employ fundamentally new technique. When generative models developed, do they still leave artifacts or even undetectable. This remain the problem for future research.

Acknowledgments

This work was supported in part by the National Natural Science Foundation of China under Grant 72434005, Grant 72225011 and Grant 72293575.

References

- [1] Midjourney. In <https://www.midjourney.com/home/>, 2022. 4, 6, 1
- [2] Wukong, 2022. 5. In <https://xihe.mindspore.cn/modelzoo/wukong>, 2022. 5. 1
- [3] Adobe. Adobe firefly. <https://firefly.adobe.com/>, 2025. Accessed: 2025-11-04. 1
- [4] Vishal Asnani, Xi Yin, Tal Hassner, and Xiaoming Liu. Reverse engineering of generative models: Inferring model hyperparameters from generated images. *IEEE Transactions on Pattern Analysis and Machine Intelligence*, 45(12):15477–15493, 2023. 3
- [5] Songran Bai, Yuheng Ji, Yue Liu, Xingwei Zhang, Xiaolong Zheng, and Daniel Dajun Zeng. Alleviating performance disparity in adversarial spatiotemporal graph learning under zero-inflated distribution. In *Proceedings of the AAAI Conference on Artificial Intelligence*, pages 11436–11444, 2025. 4
- [6] Shuanghao Bai, Wenxuan Song, Jiayi Chen, Yuheng Ji, Zhide Zhong, Jin Yang, Han Zhao, Wanqi Zhou, Wei Zhao, Zhe Li, et al. Towards a unified understanding of robot manipulation: A comprehensive survey. *arXiv preprint arXiv:2510.10903*, 2025. 4
- [7] Quentin Bammey. Synthbuster: Towards detection of diffusion model generated images. *IEEE Open Journal of Signal Processing*, 5:1–9, 2024. 6, 1
- [8] Black Forest Labs. FLUX.1: Speeding up text-to-image generation. <https://blackforestlabs.ai>, 2025. Accessed: 2025-11-26. 4
- [9] Andrew Brock et al. Large scale gan training for high fidelity natural image synthesis. In *International Conference on Learning Representations*, 2018. 1
- [10] Lucy Chai, David Bau, Ser-Nam Lim, and Phillip Isola. What makes fake images detectable? understanding properties that generalize. In *European Conference on Computer Vision*, 2020. 7
- [11] Baoying Chen, Jishen Zeng, Jianquan Yang, and Rui Yang. Drct: Diffusion reconstruction contrastive training towards universal detection of diffusion generated images. In *Forty-first International Conference on Machine Learning*, 2024. 3, 6, 2, 5
- [12] Ruoxin Chen, Junwei Xi, Zhiyuan Yan, Ke-Yue Zhang, Shuang Wu, Jingyi Xie, Xu Chen, Lei Xu, Isabel Guan, Taiping Yao, and Shouhong Ding. Dual data alignment makes ai-generated image detector easier generalizable. In *Advances in Neural Information Processing Systems*, 2025. 2, 3
- [13] Siyuan Cheng, Lingjuan Lyu, Zhenting Wang, Xiangyu Zhang, and Vikash Sehwag. Co-spy: Combining semantic and pixel features to detect synthetic images by ai. In *Proceedings of the Computer Vision and Pattern Recognition Conference*, pages 13455–13465, 2025. 3, 6, 7, 2, 5
- [14] Yunjey Choi et al. Stargan: Unified generative adversarial networks for multi-domain image-to-image translation. In *Proceedings of the IEEE Conference on Computer Vision and Pattern Recognition*, pages 8789–8797, 2018. 1
- [15] Katherine Crowson, Stefan Andreas Baumann, Alex Birch, Tanishq Mathew Abraham, Daniel Z Kaplan, and Enrico Shippe. Scalable high-resolution pixel-space image synthesis with hourglass diffusion transformers. In *Proceedings of the 41st International Conference on Machine Learning*, pages 9550–9575. PMLR, 2024. 1
- [16] Jia Deng, Wei Dong, Richard Socher, Li-Jia Li, Kai Li, and Li Fei-Fei. Imagenet: A large-scale hierarchical image database. In *2009 IEEE Conference on Computer Vision and Pattern Recognition*, pages 248–255, 2009. 3, 1
- [17] Prafulla Dhariwal et al. Diffusion models beat gans on image synthesis. *Advances in Neural Information Processing Systems*, 34:8780–8794, 2021. 1
- [18] Alexey Dosovitskiy, Lucas Beyer, Alexander Kolesnikov, Dirk Weissenborn, Xiaohua Zhai, Thomas Unterthiner, Mostafa Dehghani, Matthias Minderer, Georg Heigold, Sylvain Gelly, Jakob Uszkoreit, and Neil Houlsby. An image is worth 16x16 words: Transformers for image recognition at scale. *ICLR*, 2021. 6
- [19] R. A. Fisher. The use of multiple measurements in taxonomic problems. *Annals of Eugenics*, 7(2):179–188, 1936. 4
- [20] Google, Inc. Nano banana. <https://www.nano-banana.com/>, 2025. Accessed: 2025-08-29. 4
- [21] Shuyang Gu, Dong Chen, Jianmin Bao, Fang Wen, Bo Zhang, Dongdong Chen, Lu Yuan, and Baining Guo. Vector quantized diffusion model for text-to-image synthesis. In *Proceedings of the IEEE/CVF Conference on Computer Vision and Pattern Recognition*, pages 10696–10706, 2022. 1
- [22] Fabrizio Guillaro, Giada Zingarini, Ben Usman, Avneesh Sud, Davide Cozzolino, and Luisa Verdoliva. A bias-free training paradigm for more general ai-generated image detection. In *Proceedings of the Computer Vision and Pattern Recognition Conference (CVPR)*, pages 18685–18694, 2025. 3, 6, 2, 5
- [23] Xiao Guo, Vishal Asnani, Sijia Liu, and Xiaoming Liu. Tracing hyperparameter dependencies for model parsing via learnable graph pooling network. In *Advances in Neural Information Processing Systems*, pages 116899–116932. Curran Associates, Inc., 2024. 3
- [24] Kaiming He, Xiangyu Zhang, Shaoqing Ren, and Jian Sun. Deep residual learning for image recognition. In *Proceedings of the IEEE conference on computer vision and pattern recognition*, pages 770–778, 2016. 7
- [25] Edward J Hu, Yelong Shen, Phillip Wallis, Zeyuan Allen-Zhu, Yuanzhi Li, Shean Wang, Lu Wang, and Weizhu Chen.

LoRA: Low-rank adaptation of large language models. In *International Conference on Learning Representations*, 2022. 2, 5

[26] Yonghyun Jeong, Doyeon Kim, Seungjai Min, Seongho Joe, Youngjune Gwon, and Jongwon Choi. Bihpf: Bilateral high-pass filters for robust deepfake detection. In *2022 IEEE/CVF Winter Conference on Applications of Computer Vision (WACV)*, pages 2878–2887, 2022. 2

[27] Yuheng Ji, Yue Liu, Zhicheng Zhang, Zhao Zhang, Yuting Zhao, Xiaoshuai Hao, Gang Zhou, Xingwei Zhang, and Xiaolong Zheng. Enhancing adversarial robustness of vision-language models through low-rank adaptation. In *Proceedings of the 2025 International Conference on Multimedia Retrieval*, pages 550–559, 2025. 4

[28] Yuheng Ji, Huajie Tan, Cheng Chi, Yijie Xu, Yuting Zhao, Enshen Zhou, Huaihai Lyu, Pengwei Wang, Zhongyuan Wang, Shanghang Zhang, et al. Mathsticks: A benchmark for visual symbolic compositional reasoning with matchstick puzzles. *arXiv preprint arXiv:2510.00483*, 2025. 4

[29] Yuheng Ji, Huajie Tan, Jiayu Shi, Xiaoshuai Hao, Yuan Zhang, Hengyuan Zhang, Pengwei Wang, Mengdi Zhao, Yao Mu, Pengju An, et al. Robobrain: A unified brain model for robotic manipulation from abstract to concrete. In *Proceedings of the Computer Vision and Pattern Recognition Conference*, pages 1724–1734, 2025. 4

[30] Yuheng Ji, Yipu Wang, Yuyang Liu, Xiaoshuai Hao, Yue Liu, Yuting Zhao, Huaihai Lyu, and Xiaolong Zheng. Visualtrans: A benchmark for real-world visual transformation reasoning. *arXiv preprint arXiv:2508.04043*, 2025. 4

[31] Tero Karras et al. Progressive growing of gans for improved quality, stability, and variation. In *International Conference on Learning Representations*, 2018. 4, 6, 1

[32] Tero Karras et al. A style-based generator architecture for generative adversarial networks. In *Proceedings of the IEEE/CVF Conference on Computer Vision and Pattern Recognition*, pages 4401–4410, 2019. 1

[33] Kvikontent. Kvikontent-midjourney v6. <https://huggingface.co/Kvikontent/midjourney-v6>, 2023. 1

[34] Ouxiang Li, Jiayin Cai, Yanbin Hao, Xiaolong Jiang, Yao Hu, and Fuli Feng. Improving synthetic image detection towards generalization: An image transformation perspective. In *Proceedings of the 31st ACM SIGKDD Conference on Knowledge Discovery and Data Mining V. 1*, pages 2405–2414, 2025. 2, 6, 5

[35] Shuqiao Liang, Jian Liu, Renzhang Chen, and Quanlong Guan. Ferretnet: Efficient synthetic image detection via local pixel dependencies, 2025. 2

[36] Huan Liu, Zichang Tan, Chuangchuang Tan, Yunchao Wei, Jingdong Wang, and Yao Zhao. Forgery-aware adaptive transformer for generalizable synthetic image detection. In *Proceedings of the IEEE/CVF Conference on Computer Vision and Pattern Recognition*, pages 10770–10780, 2024. 2, 3

[37] Ze Liu, Yutong Lin, Yue Cao, Han Hu, Yixuan Wei, Zheng Zhang, Stephen Lin, and Baining Guo. Swin transformer: Hierarchical vision transformer using shifted windows. In *Proceedings of the IEEE/CVF International Conference on Computer Vision (ICCV)*, 2021. 7

[38] Zhuang Liu, Hanzi Mao, Chao-Yuan Wu, Christoph Feichtenhofer, Trevor Darrell, and Saining Xie. A convnet for the 2020s. *Proceedings of the IEEE/CVF Conference on Computer Vision and Pattern Recognition (CVPR)*, 2022. 7

[39] Ilya Loshchilov and Frank Hutter. Decoupled weight decay regularization. *arXiv preprint arXiv:1711.05101*, 2017. Submitted November 14, 2017; revised January 4, 2019. 2

[40] Simian Luo, Yiqin Tan, Suraj Patil, Daniel Gu, Patrick von Platen, Apolinário Passos, Longbo Huang, Jian Li, and Hang Zhao. Lcm-lora: A universal stable-diffusion acceleration module. *arXiv preprint arXiv:2311.05556*, 2023. 1

[41] Yunpeng Luo, Junlong Du, Ke Yan, and Shouhong Ding. Lare2: Latent reconstruction error based method for diffusion-generated image detection. In *Proceedings of the IEEE/CVF Conference on Computer Vision and Pattern Recognition (CVPR)*, pages 17006–17015, 2024. 2

[42] Huaihai Lyu, Chaofan Chen, Yuheng Ji, and Changsheng Xu. Egoprompt: Prompt pool learning for egocentric action recognition. *arXiv preprint arXiv:2508.03266*, 2025. 4

[43] Midjourney, Inc. Midjourney v6. <https://www.midjourney.com>, 2025. AI model version 6.0, Accessed: 2025-11-26. 4

[44] Alex Nichol, Prafulla Dhariwal, Aditya Ramesh, Pranav Shyam, Pamela Mishkin, Bob McGrew, Ilya Sutskever, and Mark Chen. Glide: Towards photorealistic image generation and editing with text-guided diffusion models. *arXiv preprint arXiv:2112.10741*, 2021. 1

[45] Utkarsh Ojha, Yuheng Li, and Yong Jae Lee. Towards universal fake image detectors that generalize across generative models. In *Proceedings of the IEEE/CVF Conference on Computer Vision and Pattern Recognition*, pages 24480–24489, 2023. 1, 2, 3, 6, 7, 5

[46] Jeongsoo Park and Andrew Owens. Community forensics: Using thousands of generators to train fake image detectors. In *Proceedings of the Computer Vision and Pattern Recognition Conference (CVPR)*, pages 8245–8257, 2025. 1, 3, 6, 5

[47] Taesung Park et al. Semantic image synthesis with spatially-adaptive normalization. In *Proceedings of the IEEE/CVF Conference on Computer Vision and Pattern Recognition*, pages 2337–2346, 2019. 1

[48] Pablo Pernias, Dominic Rampas, Mats Leon Richter, Christopher Pal, and Marc Aubreville. Würstchen: An efficient architecture for large-scale text-to-image diffusion models. In *The Twelfth International Conference on Learning Representations*, 2023. 1

[49] Alec Radford, Jong Wook Kim, Chris Hallacy, Aditya Ramesh, Gabriel Goh, Sandhini Agarwal, Girish Sastry, Amanda Askell, Pamela Mishkin, Jack Clark, et al. Learning transferable visual models from natural language supervision. In *International conference on machine learning*, pages 8748–8763. PMLR, 2021. 2, 6, 7

[50] Anirudh Sundara Rajan, Utkarsh Ojha, Jedidiah Schloesser, and Yong Jae Lee. Aligned datasets improve detection of latent diffusion-generated images. In *The Thirteenth International Conference on Learning Representations*, 2025. 2

[51] Robin Rombach, Andreas Blattmann, Dominik Lorenz, Patrick Esser, and Björn Ommer. High-resolution image

synthesis with latent diffusion models. In *Proceedings of the IEEE/CVF Conference on Computer Vision and Pattern Recognition (CVPR)*, pages 10684–10695, 2022. 1, 4, 6, 2

[52] Andreas Rossler et al. Faceforensics++: Learning to detect manipulated facial images. In *Proceedings of the IEEE/CVF International Conference on Computer Vision*, pages 1–11, 2019. 1

[53] Arseniy Shakhmatov, Anton Razzhigaev, Aleksandr Nikolic, Vladimir Arkhipkin, Igor Pavlov, Andrey Kuznetsov, and Denis Dimitrov. Kandinsky 2.2. <https://github.com/ai-forever/Kandinsky-2>, 2023. 1

[54] Zirui Song, Guangxian Ouyang, Mingzhe Li, Yuheng Ji, Chenxi Wang, Zixiang Xu, Zeyu Zhang, Xiaoqing Zhang, Qian Jiang, Zhenhao Chen, et al. Maniplvm-r1: Reinforcement learning for reasoning in embodied manipulation with large vision-language models. *arXiv preprint arXiv:2505.16517*, 2025. 4

[55] Chuangchuang Tan, Yao Zhao, Shikui Wei, Guanghua Gu, Ping Liu, and Yunchao Wei. Frequency-aware deepfake detection: Improving generalizability through frequency space domain learning. In *Proceedings of the AAAI Conference on Artificial Intelligence*, pages 5052–5060, 2024. 2

[56] Chuangchuang Tan, Yao Zhao, Shikui Wei, Guanghua Gu, Ping Liu, and Yunchao Wei. Rethinking the up-sampling operations in cnn-based generative network for generalizable deepfake detection. In *Proceedings of the IEEE/CVF Conference on Computer Vision and Pattern Recognition*, pages 28130–28139, 2024. 2, 6, 7, 1, 5

[57] Chuangchuang Tan, Renshuai Tao, Huan Liu, Guanghua Gu, Baoyuan Wu, Yao Zhao, and Yunchao Wei. C2p-clip: Injecting category common prompt in clip to enhance generalization in deepfake detection. In *Proceedings of the AAAI Conference on Artificial Intelligence*, pages 7184–7192, 2025. 2, 3

[58] Huajie Tan, Yuheng Ji, Xiaoshuai Hao, Xiansheng Chen, Pengwei Wang, Zhongyuan Wang, and Shanghang Zhang. Reason-rft: Reinforcement fine-tuning for visual reasoning of vision language models. In *The Thirty-ninth Annual Conference on Neural Information Processing Systems*. 4

[59] Huajie Tan, Cheng Chi, Xiansheng Chen, Yuheng Ji, Zhongxia Zhao, Xiaoshuai Hao, Yaoxu Lyu, Mingyu Cao, Junkai Zhao, Huaihai Lyu, et al. Roboos-next: A unified memory-based framework for lifelong, scalable, and robust multi-robot collaboration. *arXiv preprint arXiv:2510.26536*, 2025. 4

[60] Ming Tao, Hao Tang, Fei Wu, Xiao-Yuan Jing, Bing-Kun Bao, and Changsheng Xu. Df-gan: A simple and effective baseline for text-to-image synthesis. In *Proceedings of the IEEE/CVF conference on computer vision and pattern recognition*, pages 16515–16525, 2022. 1

[61] Ming Tao, Bing-Kun Bao, Hao Tang, and Changsheng Xu. Galip: Generative adversarial clips for text-to-image synthesis. In *Proceedings of the IEEE/CVF Conference on Computer Vision and Pattern Recognition*, pages 14214–14223, 2023. 1

[62] BAAI RoboBrain Team, Mingyu Cao, Huajie Tan, Yuheng Ji, Xiansheng Chen, Minglan Lin, Zhiyu Li, Zhou Cao, Pengwei Wang, Enshan Zhou, et al. Robobrain 2.0 technical report. *arXiv preprint arXiv:2507.02029*, 2025. 4

[63] DeciAI Research Team. Decidiffusion 2.0, 2024. 1

[64] Ashish Vaswani, Noam Shazeer, Niki Parmar, Jakob Uszkoreit, Llion Jones, Aidan N Gomez, Łukasz Kaiser, and Illia Polosukhin. Attention is all you need. In *Advances in Neural Information Processing Systems*. Curran Associates, Inc., 2017. 5

[65] Sheng-Yu Wang, Oliver Wang, Richard Zhang, Andrew Owens, and Alexei A Efros. Cnn-generated images are surprisingly easy to spot... for now. In *Proceedings of the IEEE/CVF conference on computer vision and pattern recognition*, pages 8695–8704, 2020. 2, 3, 4, 6, 1, 5

[66] Yipu Wang, Yuheng Ji, Yuyang Liu, Enshan Zhou, Ziqiang Yang, Yuxuan Tian, Ziheng Qin, Yue Liu, Huajie Tan, Cheng Chi, Zhiyuan Ma, Daniel Dajun Zeng, and Xiaolong Zheng. Towards cross-view point correspondence in vision-language models. *arXiv preprint arXiv:2512.04686*, 2025. 4

[67] Zhendong Wang, Jianmin Bao, Wengang Zhou, Weilun Wang, Hezhen Hu, Hong Chen, and Houqiang Li. Dire for diffusion-generated image detection. *arXiv preprint arXiv:2303.09295*, 2023. 2

[68] Siwei Wen, Junyan Ye, Peilin Feng, Hengrui Kang, Zichen Wen, Yize Chen, Jiang Wu, Wenjun Wu, Conghui He, and Weijia Li. Spot the fake: Large multimodal model-based synthetic image detection with artifact explanation. *arXiv preprint arXiv:2503.14905*, 2025. 2, 3

[69] Chenfei Wu, Jiahao Li, Jingren Zhou, Junyang Lin, Kaiyuan Gao, Kun Yan, Sheng ming Yin, Shuai Bai, Xiao Xu, Yilei Chen, Yuxiang Chen, Zecheng Tang, Zekai Zhang, Zhengyi Wang, An Yang, Bowen Yu, Chen Cheng, Dayiheng Liu, Deqing Li, Hang Zhang, Hao Meng, Hu Wei, Jingyuan Ni, Kai Chen, Kuan Cao, Liang Peng, Lin Qu, Minggang Wu, Peng Wang, Shuting Yu, Tingkun Wen, Wensen Feng, Xiaoxiao Xu, Yi Wang, Yichang Zhang, Yongqiang Zhu, Yujia Wu, Yuxuan Cai, and Zenan Liu. Qwen-image technical report, 2025. 1

[70] Shilin Yan, Ouxiang Li, Jiayin Cai, Yanbin Hao, Xiaolong Jiang, Yao Hu, and Weidi Xie. A sanity check for ai-generated image detection. *arXiv preprint arXiv:2406.19435*, 2024. 2, 3, 6, 7, 1, 5

[71] Zhiyuan Yan, Jiangming Wang, Peng Jin, Ke-Yue Zhang, Chengchun Liu, Shen Chen, Taiping Yao, Shouhong Ding, Baoyuan Wu, and Li Yuan. Orthogonal subspace decomposition for generalizable ai-generated image detection. *arXiv preprint arXiv:2411.15633*, 2024. 3, 7

[72] Yongqi Yang, Zhihao Qian, Ye Zhu, Olga Russakovsky, and Yu Wu. D3: Scaling up deepfake detection by learning from discrepancy. In *Proceedings of the IEEE/CVF Conference on Computer Vision and Pattern Recognition*, 2025. 1, 3, 6, 7, 2, 5

[73] Haifeng Zhang, Qinghui He, Xiuli Bi, Weisheng Li, Bo Liu, and Bin Xiao. Towards universal ai-generated image detection by variational information bottleneck network. In *Proceedings of the Computer Vision and Pattern Recognition Conference*, pages 23828–23837, 2025. 3

- [74] Jun-Yan Zhu et al. Unpaired image-to-image translation using cycle-consistent adversarial networks. In *Proceedings of the IEEE International Conference on Computer Vision*, pages 2223–2232, 2017. [1](#)
- [75] Mingjian Zhu, Hanting Chen, Qiangyu Yan, Xudong Huang, Guanyu Lin, Wei Li, Zhijun Tu, Hailin Hu, Jie Hu, and Yunhe Wang. Genimage: A million-scale benchmark for detecting ai-generated image. *Advances in Neural Information Processing Systems*, 36:77771–77782, 2023. [4](#)
- [76] Mingjian Zhu, Hanting Chen, Qiangyu Yan, Xudong Huang, Guanyu Lin, Wei Li, Zhijun Tu, Hailin Hu, Jie Hu, and Yunhe Wang. Genimage: A million-scale benchmark for detecting ai-generated image. *Advances in Neural Information Processing Systems*, 36, 2024. [3](#), [6](#), [1](#)

Scaling Up AI-Generated Image Detection via Generator-Aware Prototypes

Supplementary Material

We organize the supplementary in the following way:

- Sec. A: Detailed information of the introduced series of dataset build in previous section.
- Sec. B: Details of the 6 selected benchmarks.
- Sec. C: Introduction to the selected baselines.
- Sec. D: Detailed results of each test subsets.
- Sec. E: Implementation details of the proposed method.
- Sec. F: Additional derivation and analysis.
- Sec. G: Future perspectives towards reasoning-driven and embodied forensics.

A. Settings of the toy dataset

In Sec.3, we introduce a series of datasets, comprising generated images from different numbers of generators. In this section we will give the constructing procedure of these datasets.

First, there are 8 generators in GenImage [76] dataset, in each generator subset, there are 1000 types of object mirroring the 1000 categories of ImageNet-1k [16]. We select generator subset composed of n_g generators based on Tab. 5. For each of the 1000 categories, we randomly sample n_s images in each generator subset. To pair real images, we randomly sample $n_s \times n_g$ images from the original ImageNet dataset. n_s is determined via $1000 \times n_s \times n_g = 8000$.

For the last dataset, which consist of thousands of generators, we leverage Community-Forensics training dataset [46] for collecting, which is the same as our training dataset. we randomly sample 2 images from each generator in it, which consist of about 9000 generated images. Then we randomly sample 8,000 real images as before to construct the last dataset in the series.

group	n_g	Generator(s)
1	1	SDv1.4
2	2	SDv1.4, BigGAN
3	4	SDv1.4, BigGAN, VQDM, Glide
4	8	All GenImage

Table 5. Generators used to build our datasets.

B. Benchmarks

We select 6 benchmarks to represent most existed generative models to evaluate the methods. Though some subsets have same or similar architecture, their training condition, sampling strategy and semantic content are not quite the same. Thus we preserve all subsets that have same name to simulate a variety of generated images.

Forensic Synthetic [65] contains a series of CNN-generated images, we select its GAN variants, including ProGAN [31], StyleGAN [32], StyleGAN2, CycleGAN [74], StarGAN [14], GauGAN [47], BigGAN [9], and Deepfake [52] for forgery face.

UFD [45] datasets expand the dataset above by introducing several early diffusion models and commercial APIs, including latent diffusion model [51], Glide [44] and Guided [17] diffusion model.

GenImage [76] provide a dataset trained on ImageNet-1k. It has 8 generative models in both GANs, Diffusion Models and Commercial APIs, including BigGAN [9], VQDM [21], Stable Diffusions, Wukong [2], ADM [17] and Midjourney [1].

SynthBuster [7] provide an aligned dataset, where real images and generated images are all in PNG format, which makes it challenging for AIGI detectors that leverage format shortcut. Moreover the generated images are also from popular latent diffusions, including DALL-E, Stable Diffusions, Firefly[3] and Glide.

Chameleon [70] provides a sanity check for AI-generated image detection. They build a high quality dataset where generated images are source from internet and some unknown source. All images in this benchmark are said to be indistinguishable by human. Since all images are gather from the unknown source, there's only one subset in this benchmark.

Community Forensics Evaluation Set [46] is build to evaluate the model's ability to generalize to unseen generators that trained in Community Forensics dataset. This evaluation dataset is also the most up-to-date dataset, containing generators like Deci Diffusion V2 [63], GALIP [61], KandinskyV2.2 [53], Kvikontent [33], LCM-LoRA-SDv1.5, LCM-LoRA-SDXL, LCM-LoRA-SSD1B [40], Stable Cascade [48], DF-GAN [60], and HDiT [15].

Above all, we have 55 subsets for testing. Given the large scale of our training data, the training domain overlaps with several previously constructed datasets. Consequently, our evaluation comprises 29 completely unseen generator subsets, the rest, even though seen in training set, still have a different generated condition. Sample images from the test set are shown in Fig. 8.

Metrics. Following prior works [45, 56, 65], we compute a threshold-free metric, mean average precision (AP), and a threshold-based metric, binary accuracy (Acc). When



Figure 8. Examples of test subsets, we visualize some in-domain datasets with our training set along with some out-of-distribution sets.

computing accuracy, the threshold was set to 0.5.

C. Baselines

In this section, we will give a brief introduction to the baselines for comparison.

C.1. GAN-Generalized

CNNDetection [65] uses a ResNet-50 as a classifier with data augmentation to detect CNN-generated images. **NPR** [56] rethink up-sampling operation in most generative architecture and detect them via a interpolation pattern. **UniFD** [45] leverage the image encoder of CLIP for feature extraction, it takes image embeddings for classification with simple KNN or linear layer. **SAFE**[34] extracts high frequency band as artifact with various data augmentation to build a CNN classifier. **AIDE** uses a hybrid feature of both CLIP image embedding , high and low frequency patches via DCT scoring, and concatenate them for final decision. These baselines are all trained on GAN generated images provided by the training set of CNNDetection [65].

C.2. Diffusion-Generalized

In the diffusion era [51], more method aim to detect generated images with a more realistic diffusion generated images. **DRCT** [11] construct a diffusion reconstruct dataset and used it to train a classifier with classification objective and contrastive learning objective. We use its Conv-B variant trained on SDv2.1. **Co-SPY** [13] also uses a hybrid feature for classification, but a combination of CLIP embedding and VAE-reconstruct residual. **B-Free** [22] proposed a paradigm that generated images should come from inpainting models rather than unconditional generators or T2Is to prevent semantic bias. It trained an end-to-end classifier with proposed dataset.

C.3. Scaling-Ups

Scaling up detectors use a training dataset from a more diverse source. To solve the sanity check for AIGI detection, **AIDE** [70] provide another checkpoint that trained a classifier with all images in GenImage, including both GANs and Diffusions. **D3** [72] proposed a dual feature extraction branch, a original image and a patch-shuffled image to learn comprehensive traces, it uses a training dataset consist of GenImage and CNNDetection. Community Forensics construct a large dataset with thousands of generators and use it to train classifier with a standard ViT.

D. Detailed results of experiments

The following tables show detailed results for the selected 6 benchmarks. All baselines are evaluated with their provided checkpoints. Tab. 6 shows results of ForenSynths, Tab. 7 shows results of UFD, Tab. 8 shows results of GenImage, Tab. 9 shows results of SynthBuster, Tab. 10 and Tab. 11 shows results of Community Forensics evaluation set.

E. Implementation Details

To validate the reproducibility, we present our implementation details in this section.

Network Design The image encoder we use is CLIP:ViT-L with a patch size of 14×14 . The MLP is composed of two hidden layer with dimensions $1024 \rightarrow 128 \rightarrow 1$. In the second stage, we discard the second layer to make the MLP $1024 \rightarrow 128$, then we apply LoRA [25] in q_proj , k_proj , v_proj of image encoder with LoRA parameter $r = 16$, $\alpha = 32$, $dropout = 0.1$.

Training For image in training set, we apply Random-Crop to 224×224 , and to those image whose resolution is smaller than this, we apply 0-padding to make it enough to crop. We automatically separate 5% samples of dataset to form a validation set. We use AdamW [39] optimizer with

a learning rate of 10^{-4} and a weight decay of 0.01 in the two stages. In the first stage, training last for 20 epochs. In the second stage, we train until the validation accuracy reaches 99.9% or do not improve for 3 epochs to prevent performance degradation.

Testing For images in testing sets, we apply CenterCrop to 224×224 , which is the same as most baselines, except for **B-Free**, who uses a resolution of 504×504 and **Co-SPY** uses a 384×384 , to best excel their performance, we did not modify their model but directly report their performance on original resolution.

F. Additional Derivation and Analysis

In this section, we provide supplementary materials to substantiate the claims made in the main text. Specifically, we present a rigorous mathematical derivation modeling the data heterogeneity in scaling-up settings (Sec. F.1) and offer qualitative visualizations of the attention maps to demonstrate how our method alters the encoder’s focus (Sec. F.2).

F.1. Detailed Derivation of Theory

Recall that in Sec. 3 of the main paper, we identified the “Benefit then Conflict” dilemma, attributing it to the severe data-level heterogeneity that arises when aggregating multiple generators. To theoretically quantify this phenomenon, we model the distribution of real and generated images and analyze the behavior of feature variance.

Why GMM? How to calculate variance in GMM?

We adopt the Gaussian Mixture Model (GMM) as a proxy for the real-world data distribution. This choice is motivated by the structure of commonly used datasets like ImageNet, which consist of distinct categories. Specifically, we model the image features within each category as a multivariate Gaussian distribution. While this is a simplified assumption, it remains theoretically robust and yields conclusions consistent with more complex scenarios. The total variance of the generated distribution is derived as follows:

$$\Sigma_{gen} = \mathbb{E}_G [\text{Var}(X|G)] + \text{Var}_G [\mathbb{E}(X|G)], \quad (11)$$

For the i -th generator, its variance is computed by:

$$\begin{aligned} \text{Var}(X|G = i) &= \Sigma_{gen}^i \\ &= \sum_{j=1}^M \pi_{i,j} \Sigma_{i,j} + \sum_{j=1}^M \pi_{i,j} (\mu_{i,j} - \mu_i) (\mu_{i,j} - \mu_i)^T \end{aligned} \quad (12)$$

Thus, the total variance can be expressed as:

$$\begin{aligned} \Sigma_{gen} &= \sum_i^G w_i \sum_j^M \pi_{i,j} \Sigma_{i,j} \\ &+ \sum_i^G w_i \sum_j^M \pi_{i,j} (\mu_{i,j} - \bar{\mu}) (\mu_{i,j} - \bar{\mu})^T \\ &+ \sum_i^G w_i (\mu_i - \bar{\mu}) (\mu_i - \bar{\mu})^T \\ &= \underbrace{\mathbb{E}_M [\text{Var}(X|G_i, M)|G_i] + \text{Var}_M [\mathbb{E}(X|G_i, M)|G_i]}_{\text{generator fitting variance}} \\ &+ \underbrace{\text{Var}_G [\mathbb{E}(X|G)]}_{\text{cross generator variance}}, \end{aligned} \quad (13)$$

where $\mu_i = \sum_j^M \pi_{i,j} \mu_{i,j}$, and $\bar{\mu} = \sum_i^G \mu_i$ denotes the mean within a generator and the global mean across the entire dataset, respectively.

How do prototypes limit variance growth?

Having established that variance increases with generator diversity, we now show how our prototype mapping strategy mitigates this issue. In prototype mapping, the feature embedding is reorganized into a linear combination of prototypes; this operation effectively sets an upper bound on the embedding’s variance.

We have $\tilde{f} = \sum w_i v_i$ where w_i is the attention score and v_i is a prototype vector. Let F be the random variable of this reorganized embedding. Its variance is given by:

$$\text{Var}(F) = \mathbb{E} [||F - \mathbb{E}(F)||^2], \quad (14)$$

where $\text{Var}(\cdot)$ here denotes its trace in the covariance matrix, i.e., $\text{tr}(\Sigma)$. To proceed, we introduce an independent identically distributed random variable F' to reformulate this term as:

$$\begin{aligned} \text{Var}(F) &= \frac{1}{2} \mathbb{E} [||F - F'||^2] \\ &= \frac{1}{2} \sum w_i w_j ||v_i - v_j||^2, \end{aligned} \quad (15)$$

Assume $D = \max_{v \in P} ||v_i - v_j||$. Since all the prototypes are determined and fixed, this maximum distance is a constant. Due to the fact that $w_i, w_j \in [0, 1]$ and $\sum w_i = 1$, this variance term can be bounded by:

$$\text{Var}(F) \leq \frac{1}{4} D^2. \quad (16)$$

This derivation confirms that regardless of the number of source generators, the variance of the features mapped to the prototype space remains bounded by the geometry of the prototype set.

F.2. Visualization of Attention Maps

To provide interpretability for our model’s performance, we move beyond theoretical bounds to empirical visualization. We compare the attention maps from both the original CLIP image encoder and the encoder fine-tuned by our proposed GAPL.

These attention maps represent the attention scores between the [CLS] token and all spatial patch tokens. The image encoder consists of 24 ViT blocks; in our visualization, we sample 8 blocks, with block indices ascending from left to right (shallow to deep). For visual clarity, bicubic interpolation is applied to the raw attention maps. As shown in Fig. 9 and Fig. 10, the comparisons demonstrate two key findings: (1) Our encoder preserves rich semantic information in the shallow layers, maintaining the generalization capability of the pre-trained model; (2) In deeper layers, compared to the original CLIP, our model effectively leverages more patches to form a more comprehensive artifact pattern. Visually, this manifests as more pronounced and focused bright spots in the deeper layers, indicating that GAPL has successfully learned to attend to generator-specific traces.

G. Future Perspectives

While our proposed GAPL framework achieves state-of-the-art performance by managing data heterogeneity through generator-aware prototypes, we recognize that the arms race between generation and detection is evolving. As generative models (e.g., Flux [8], Midjourney v6 [43], Nano Banana Pro [20]) increasingly mitigate low-level statistical artifacts, relying solely on texture or frequency cues may face diminishing returns. We envision that the next generation of AIGI detectors must integrate higher-level cognitive capabilities. Specifically, we identify three promising avenues where our scaling-up principles can intersect with broader AI domains:

From Artifact Detection to Visual Reasoning. Current forensic methods predominantly focus on signal-level anomalies. However, highly realistic AI-generated images often retain subtle *semantic* or *logical* inconsistencies (e.g., impossible shadows, mismatched reflections, or counting errors) that are invisible to standard classifiers. Future work should explore integrating **Visual Reasoning** frameworks [28, 30, 54, 58] into the detection pipeline. By leveraging neuro-symbolic approaches or chain-of-thought reasoning, a detector could move beyond binary classification to provide interpretable evidence based on compositional logic, effectively identifying “why” an image violates reality even when pixel statistics appear perfect.

Incorporating Spatial Intelligence and Physical Constraints. A persistent weakness in current generative

models is their frequent violation of 3D geometry and physical laws. While GAPL effectively learns 2D prototypes, it does not explicitly model the underlying 3D structure of the scene. Incorporating spatial intelligence [29, 62, 66] could serve as a powerful orthogonal check. Models equipped with 3D-aware representations or spatial reasoning capabilities can detect geometric implausibilities—such as “Escher-like” structures or inconsistent depth cues—that purely 2D generative models fail to resolve. This aligns with our observation of “Benefit then Conflict,” suggesting that physical laws could serve as the ultimate invariant feature across diverse generators.

Trustworthy Perception in Embodied AI. Finally, the utility of AIGI detection extends beyond digital media forensics into the physical world. As we deploy autonomous agents, ensuring trustworthy perception is critical. Embodied agents operating in the real world must distinguish between authentic sensory inputs and potentially manipulated streams (e.g., adversarial projections or deepfakes in video feeds) [5, 27]. Furthermore, robust detection models like GAPL can act as quality filters for Embodied AI [6, 30, 42, 59], particularly in Sim-to-Real pipelines where agents are trained on synthetic data. By rigorously curating high-fidelity synthetic data that adheres to physical realism, we can ensure that embodied agents develop robust representations that generalize better to physical reality.

Method	ProGAN		StyleGAN		StyleGAN2		StarGAN		GauGAN		CycleGAN		BigGAN		Deepfake		Mean	
	Acc	AP	Acc	AP	Acc	AP	Acc	AP	Acc	AP	Acc	AP	Acc	AP	Acc	AP	Acc	AP
CNNDet [65]	100.0	100.0	74.3	98.4	76.3	92.1	81.1	95.3	80.1	98.0	81.1	96.4	59.5	88.2	51.0	66.1	75.3	91.8
NPR [56]	99.8	99.9	97.3	99.9	99.5	100	99.7	100	79.1	80.2	94.5	97.6	83.6	84.7	73.7	72.5	90.1	91.8
UniFD [45]	99.8	100.0	85.4	97.5	74.5	97.6	96.0	99.5	99.4	100.0	98.3	99.8	94.7	99.2	67.5	80.3	89.4	96.7
SAFE [34]	99.8	100.0	97.6	99.8	98.7	100.0	99.8	100.0	92.2	96.9	99.1	99.8	89.5	95.1	93.2	97.2	96.2	98.6
AIDE [70]	96.3	99.8	97.2	99.7	98.1	99.8	98.4	99.9	76.9	96.0	95.6	99.4	78.3	96.7	54.2	68.7	86.8	95.0
DRCT [11]	50.2	50.2	49.1	49.1	49.3	45.3	38.3	38.7	49.9	43.2	49.3	44.6	49.7	47.8	64.7	78.4	50.1	49.6
Co-SPY [13]	74.7	78.1	63.7	69.8	59.7	62.9	62.1	94.3	69.6	83.4	58.5	55.8	71.6	83.9	64.9	78.7	65.6	75.9
B-Free [22]	95.6	99.3	74.8	93.6	71.1	89.4	81.1	93.5	96.0	99.8	65.4	90.5	91.5	98.9	73.7	89.2	81.2	94.3
AIDE [†] [70]	92.7	98.8	88.6	95.1	93.6	98.6	88.0	99.0	87.7	98.9	92.0	98.9	84.9	97.7	54.8	63.2	85.3	93.8
D3 [72]	99.8	100.0	93.5	99.1	95.8	99.5	93.5	98.7	98.7	100.0	95.9	99.5	99.6	100.0	67.5	87.0	93.0	98.0
CommForen [46]	92.8	99.8	93.1	99.3	92.7	99.5	98.8	99.9	98.8	99.9	95.5	99.8	99.6	100.0	66.8	88.9	92.2	98.2
GAPL(Ours)	99.9	100.0	98.1	100.0	99.5	100.0	97.0	99.9	99.6	100.0	98.2	99.9	98.6	100.0	88.2	96.8	97.2	99.5

Table 6. Detaild results on the benchmark ForenSynth [65]. we only select its GAN variant. AIDE[†] denotes its scaling up checkpoint trained on 8 generators.

Method	DALL-E		Glide-50-27		Glide-100-10		Glide-100-27		Guided		LDM-100		LDM-200		LDM-200-cfg		Mean	
	Acc	AP	Acc	AP	Acc	AP	Acc	AP	Acc	AP	Acc	AP	Acc	AP	Acc	AP	Acc	AP
CNNDet [65]	52.9	68.4	55.7	78.0	54.3	74.3	53.3	73.7	52.8	68.1	52.0	68.7	51.5	68.2	52.2	69.6	53.1	71.1
NPR [56]	90.3	97.4	97.2	99.2	97.6	99.2	96.9	99.1	87.1	92.6	97.4	99.1	97.6	99.2	97.4	99.0	95.2	98.1
UniFD [45]	87.5	97.7	79.2	96.0	78.0	95.5	78.7	95.8	70.0	88.3	95.2	99.3	94.5	99.4	74.2	93.2	82.2	95.7
SAFE [34]	97.5	99.7	96.6	99.2	97.3	99.4	95.8	98.9	82.4	95.8	98.8	100.0	98.8	100.0	98.7	99.9	95.7	99.1
AIDE [70]	89.7	99.6	89.9	99.8	89.8	99.6	89.9	99.8	94.2	98.9	90.1	99.9	90.1	99.9	90.1	99.9	90.5	99.7
DRCT [11]	55.6	57.8	56.2	62.6	61.0	70.4	56.2	62.7	62.6	89.3	88.8	96.6	88.9	96.7	90.3	97.5	70.0	79.2
Co-SPY [13]	81.8	87.2	69.0	74.6	76.7	81.7	73.5	78.2	62.7	87.4	82.7	86.9	83.1	87.5	85.2	91.0	76.8	84.3
B-Free [22]	93.2	97.9	78.6	90.2	81.8	91.9	77.9	89.4	74.6	93.6	97.2	99.9	97.1	99.8	96.9	99.8	87.1	95.3
AIDE [†] [70]	98.7	99.9	99.0	100.0	99.1	100.0	99.0	100.0	95.5	99.9	99.1	100.0	99.1	100.0	99.1	100.0	98.6	100.0
D3 [72]	94.0	98.7	95.8	99.3	95.8	99.4	95.7	99.5	95.9	99.6	96.1	99.7	95.8	99.7	89.3	96.5	94.8	99.0
CommForen [46]	98.4	99.9	97.1	99.6	98.2	99.8	96.8	99.6	66.1	76.6	98.5	99.9	98.7	99.9	98.5	99.9	94.0	96.9
GAPL(Ours)	97.8	100.0	97.7	99.9	97.8	100	97.7	100.0	93.4	98.6	97.8	100.0	97.9	100.0	97.9	100	97.2	99.8

Table 7. Detaild results on the benchmark UFD. We refer this set to the diffusion part that [45] added.

Method	VQDM		SDv1.4		BigGAN		Wukong		SDv1.5		Glide		Midjourney		ADM		Mean	
	Acc	AP	Acc	AP	Acc	AP	Acc	AP	Acc	AP	Acc	AP	Acc	AP	Acc	AP	Acc	AP
CNNDet [65]	52.1	68.8	50.5	59.8	51.2	78.6	50.8	59.3	50.7	60.6	52.3	67.6	51.3	64.7	51.5	65.6	51.3	65.6
NPR [56]	89.6	94.1	92.1	95.0	70.1	80.3	88.0	93.0	91.7	95.4	93.2	96.5	79.7	86.5	85.7	91.7	86.2	91.6
UniFD [45]	84.0	96.3	64.1	87.4	89.8	98.5	71.8	91.2	64.4	86.0	61.6	84.6	57.2	75.5	67.1	86.8	70.0	88.3
SAFE [34]	96.1	99.6	99.4	100.0	97.6	99.8	98.1	99.8	98.8	99.9	97.2	99.6	95.5	99.5	81.5	96.4	95.5	99.3
AIDE [70]	98.4	99.9	98.3	99.9	98.9	99.9	97.3	99.8	98.1	99.8	98.6	99.9	86.4	96.6	96.8	99.5	96.6	99.4
DRCT [11]	61.3	85.4	97.9	99.8	52.3	86.3	95.9	99.6	97.9	99.8	60.1	91.2	98.2	99.9	60.0	90.2	78.0	94.0
Co-SPY [13]	72.2	93.9	93.1	99.2	64.7	90.8	91.2	98.8	93.0	99.0	81.4	96.5	70.0	91.0	58.8	84.3	78.0	94.2
B-Free [22]	88.2	98.3	99.4	100.0	76.5	96.8	99.4	100.0	99.3	100.0	69.7	93.8	94.1	99.3	72.5	93.7	87.4	97.7
AIDE [†] [70]	99.9	100.0	99.8	100.0	99.9	100.0	99.6	100.0	99.8	100.0	99.8	100.0	99.0	100.0	99.5	100.0	99.7	100.0
D3 [72]	98.3	99.9	98.1	99.8	97.1	99.7	97.7	99.8	97.7	99.8	98.3	99.8	79.7	95.8	96.8	99.6	95.5	99.3
CommForen [46]	90.9	99.7	90.6	99.2	71.5	81.6	91.0	99.1	90.5	99.2	89.4	98.4	77.5	86.8	72.9	83.5	84.3	93.4
GAPL(Ours)	98.2	100	98.2	100	97.9	99.8	98.1	99.9	98.0	99.9	98.1	99.9	90.3	97.6	95.0	99.2	96.7	99.6

Table 8. Detaild results on the benchmark GenImage.

Method	Real	DALLE-2		Firefly		SDv1.4		SDXL		DALLE-3		Glide		MJ-v5		SDv1.3		SDv2		Mean	
	Acc	Acc	AP	Acc	AP	Acc	AP	Acc	AP	Acc	AP	Acc	AP	Acc	AP	Acc	AP	Acc	AP	Acc	AP
CNNDet [65]	96.5	7.0	64.8	14.4	74.9	1.5	49.9	5.2	59.0	0.1	36.2	1.8	46.9	1.2	44.8	1.3	49.3	4.8	96.5	50.3	54.0
NPR [56]	5.6	98.4	49.6	5.2	33.3	94.3	50.6	100	54.7	15.5	31.0	91.6	50.8	80.5	46.1	94.3	50.0	70.4	42.7	38.9	45.4
UniFD [45]	93.5	77.0	95.2	86.0	97.4	45.6	85.3	41.4	83.5	0.7	41.2	11.5	63.5	10.4	61.0	44.8	85.3	58.6	89.9	67.6	78.0
SAFE [34]	15.5	92.0	42.2	4.3	31.0	91.8	55.9	87.4	37.1	44.5	34.7	58.1	36.0	97.0	54.8	91.0	53.9	99.5	56.5	44.7	44.7
AIDE [70]	66.7	45.7	57.0	0.0	30.8	95.1	94.8	98.2	94.3	2.8	35.9	96.7	95.7	75.3	80.3	95.8	95.3	95.6	93.3	67.0	75.3
DRCT [11]	96.1	4.1	53.6	11.4	60.7	88.2	97.9	89.6	98.2	35.6	80.8	14.1	72.9	99.4	99.9	89.6	98.2	99.9	100.0	77.6	84.7
Co-SPY [13]	97.6	48.5	90.8	43.6	87.5	74.7	96.4	44.1	87.9	73.7	96.5	80.6	97.8	35.2	85.0	74.5	96.7	40.0	85.4	77.4	91.6
B-Free [22]	98.5	88.5	98.9	99.2	99.9	99.8	99.9	100.0	100.0	93.1	99.4	42.7	91.8	98.9	99.9	100.0	100.0	99.5	99.9	94.9	98.9
AIDE [†] [70]	32.8	27.3	35.8	0.3	31.5	99.0	64.4	98.6	64.8	34.8	43.4	97.1	66.8	98.6	75.0	99.7	65.8	96.7	57.0	52.7	56.0
D3 [72]	82.0	87.7	92.6	92.0	95.3	96.5	97.9	89.4	93.6	28.6	61.3	90.6	95.3	62.6	81.2	96.4	97.7	82.6	90.8	81.3	89.5
CommForen [46]	84.6	83.9	91.6	93.1	96.6	94.7	97.4	98.5	98.3	76.1	88.4	90.0	96.0	80.6	91.4	95.7	97.7	92.9	95.3	87.1	94.8
GAPL(Ours)	90.0	94.0	97.5	94.3	98.2	98.1	99.3	99.8	99.8	60.1	85.3	97.6	99.2	92.0	97.4	98.2	99.3	96.4	98.7	91.1	97.2

Table 9. Detailed results on the benchmark SynthBuster [7]. In this benchmark, all generated images are pair with exactly the same real images. Thus we report the real images accuracy and each generator's fake accuracy independently. We pair the metrics of real and each generators to get the final mean metrics .

Method	DFGAN		MJv6		Kandinsky		SDcas.		MJv5		Firefly2		Firefly3		GALIP		LCM-lora-sdxl		Hourglass		Kvikontent	
	Acc	AP	Acc	AP	Acc	AP	Acc	AP	Acc	AP	Acc	AP	Acc	AP	Acc	AP	Acc	AP	Acc	AP	Acc	AP
NPR [56]	96.6	100.0	98.6	99.0	57.7	56.1	57.4	56.4	96.7	98.3	49.2	45.0	49.6	52.4	51.7	48.0	39.9	41.6	88.6	91.6	58.6	56.3
SAFE [34]	50.3	44.8	49.9	45.0	49.6	53.2	49.9	51.0	49.9	45.1	50.0	51.3	50.1	51.2	49.5	53.9	49.5	52.3	50.1	45.2	50.2	51.5
AIDE [70]	49.9	43.9	49.8	44.7	49.9	50.1	50.2	52.6	49.9	44.4	50.2	46.2	50.2	46.8	49.7	53.0	49.7	46.1	49.8	46.1	50.1	54.1
DRCT [11]	49.9	45.9	49.6	47.0	49.6	53.1	49.4	52.7	49.7	50.5	49.6	49.1	49.9	47.0	50.2	56.6	50.0	49.0	50.0	46.9	49.6	52.2
Co-SPY [13]	50.0	84.5	70.1	86.5	68.4	74.8	71.0	76.7	63.0	80.8	68.6	86.4	86.7	95.8	38.4	34.1	43.1	38.8	52.8	59.1	74.4	84.8
B-Free [22]	92.2	96.5	76.7	84.9	85.7	99.4	86.1	99.3	86.2	97.2	82.9	92.7	81.8	91.7	81.8	91.9	85.0	97.6	57.6	65.6	86.6	99.5
AIDE [†] [70]	49.9	56.4	49.7	46.9	50.4	53.3	50.8	53.8	50.2	47.5	49.7	50.7	50.0	47.8	50.4	55.9	50.4	51.8	50.0	44.7	50.3	48.1
D3 [72]	98.4	100.0	69.5	81.0	67.9	84.5	71.5	90.0	76.7	87.0	80.0	90.8	78.6	88.7	70.8	90.8	63.0	77.7	68.3	83.1	74.9	95.7
GAPL(Ours)	99.0	100	87.1	97.3	93.0	99.1	93.3	99.6	88.6	99.3	87.3	96.2	85.1	93.7	90.6	98.1	88.2	95.8	78.5	89.4	94.5	99.8

Table 10. Detailed results on the benchmark Community forensic evaluation. This is the first part. Note that the results of CNNDet, UniFD and CommForen are directly cited from the original paper [46] and dataset repository, whose detailed results are not available.

Method	DALL-E 2		DALL-E 3		LCM-lora-sdvl1.5		DeciDiff.		FLUX-dev		FLUX-schnell		IdeogramV2		IDeogramV1		Imagen3		LCM-lora-ssd1b		Mean	
	Acc	AP	Acc	AP	Acc	AP	Acc	AP	Acc	AP	Acc	AP	Acc	AP	Acc	AP	Acc	AP	Acc	AP	Acc	AP
NPR [56]	91.7	97.6	96.5	99.2	53.6	50.1	43.9	44.1	98.1	98.9	97.8	99.0	96.4	98.8	96.5	98.5	98.6	98.7	32.3	38.4	73.8	74.7
SAFE [34]	50.7	44.8	50.1	45.1	49.7	50.8	49.7	50.5	49.9	45.1	50.1	45.0	50.1	45.0	49.9	45.1	50.1	44.9	50.0	53.2	50.0	48.3
AIDE [70]	49.6	44.2	50.0	45.2	50.1	52.4	50.0	48.5	49.9	44.9	49.8	44.5	50.0	44.4	49.9	44.7	49.8	45.0	50.0	47.7	49.9	47.1
DRCT [11]	49.3	46.8	49.5	49.0	49.8	51.5	49.6	51.8	48.4	46.8	48.6	47.0	50.0	49.1	49.6	49.4	49.0	49.0	49.2	46.9	49.5	49.4
Co-SPY [13]	77.4	91.3	85.2	96.0	67.2	74.1	71.7	79.8	80.1	93.5	71.8	87.6	71.2	88.3	75.6	90.8	77.0	91.8	61.0	68.3	67.9	79.2
B-Free [22]	74.3	81.3	86.5	98.9	85.5	99.0	86.0	99.3	73.8	82.7	79.0	88.2	81.2	89.2	81.8	91.4	74.6	83.0	87.0	98.2	81.5	91.8
AIDE [†] [70]	49.3	47.4	49.9	45.1	50.6	48.2	50.4	50.7	49.9	40.9	50.1	41.7	50.0	42.9	50.0	43.7	50.1	44.4	50.0	51.8	50.1	48.3
D3 [72]	87.5	95.0	90.1	96.6	67.0	80.6	62.1	76.4	79.3	89.7	73.5	83.8	67.2	77.5	67.6	78.6	70.7	83.1	61.5	74.5	73.6	86.0
GAPL(Ours)	88.4	97.5	88.9	99.6	93.9	99.7	92.3	99.1	87.3	98.9	88.0	98.2	88.0	98.2	87.7	98.7	87.0	95.9	90.4	97.6	89.4	97.8

Table 11. Detailed results on the benchmark Community forensic evaluation. This is the second part.

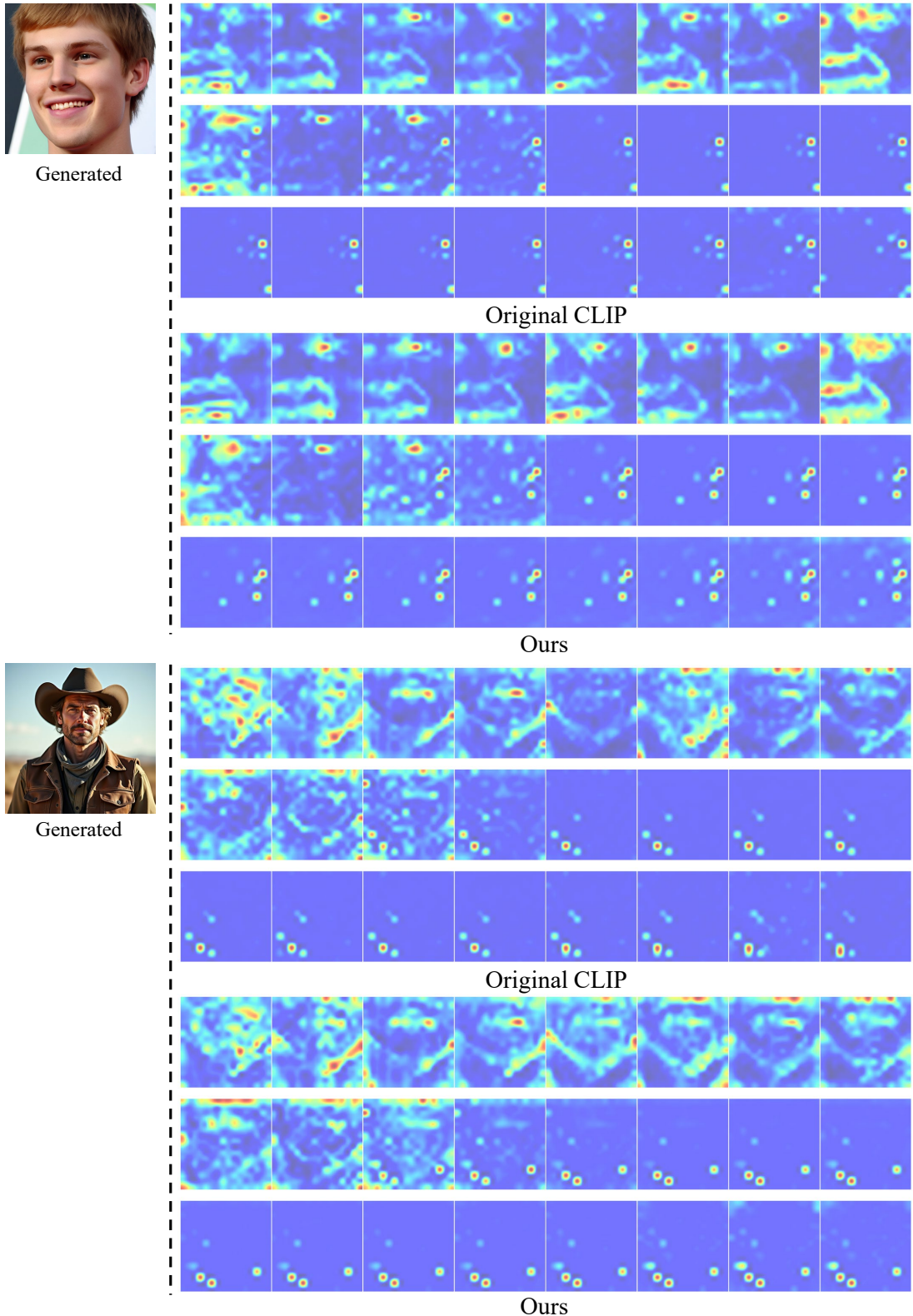


Figure 9. **Self-Attention map** between original CLIP backbone and our finetuned backbone. There are 24 ViT blocks in the image encoder, we plot 8 blocks in each row, with indices increasing from left to right. For clarity of visualization, we use bicubic interpolation between image patches. In the shallow layers, we preserve most semantic features, in deep layers, our attention includes a wider range compared to original CLIP.

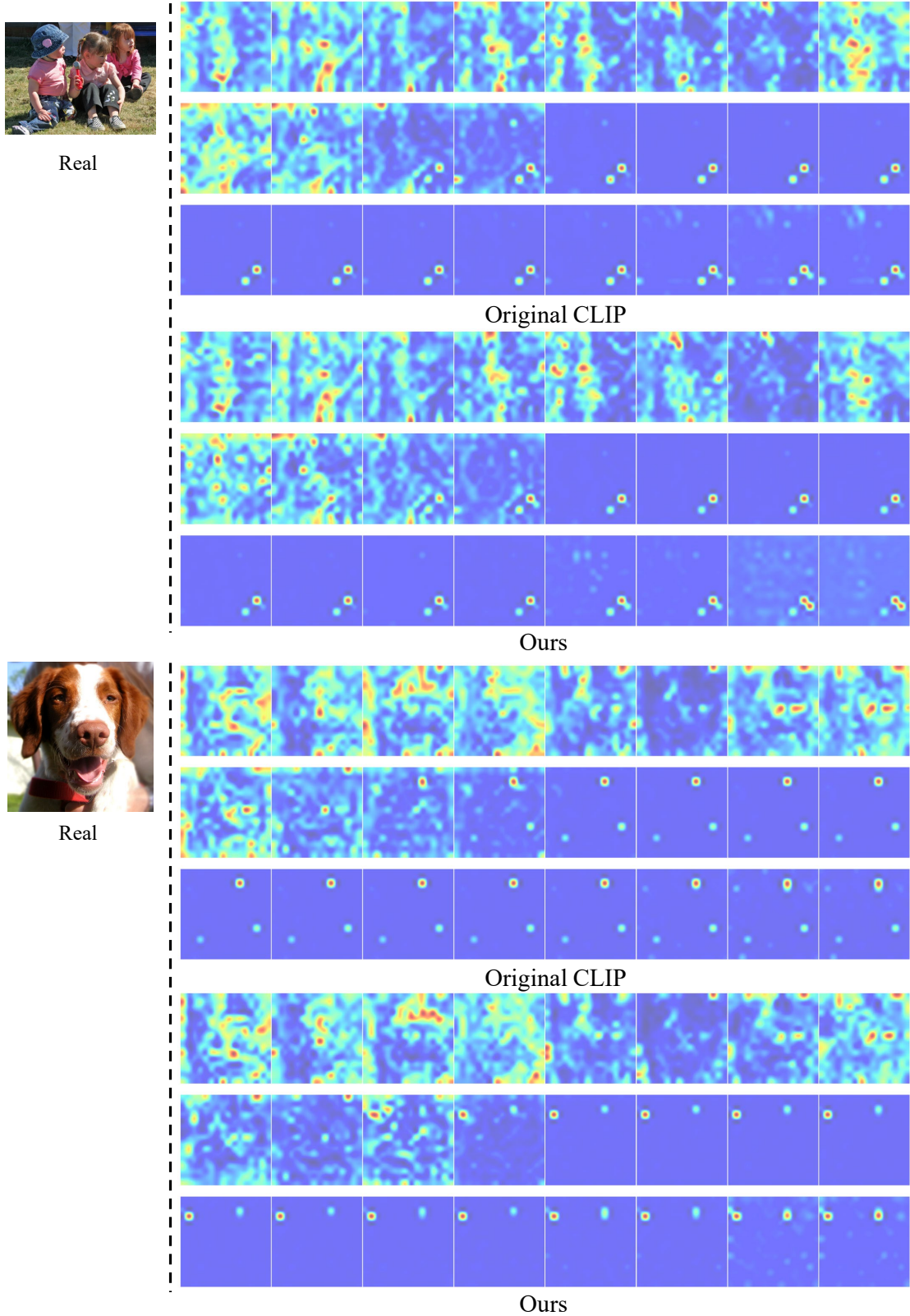


Figure 10. **Self-Attention map** between original CLIP backbone and our finetuned backbone. There are 24 ViT blocks in the image encoder, we plot 8 blocks in each row, with indices increasing from left to right. For clarity of visualization, we use bicubic interpolation between image patches. In the shallow layers, we preserve most semantic features, in deep layers, our attention includes a wider range compared to original CLIP.